Powder Technology 329 (2018) 129–136

Contents lists available at ScienceDirect

Powder Technology

journal homepage: www.elsevier.com/locate/powtec

Microfluidic production of endoskeleton droplets with controlled size and shape

Marco Caggioni[a], Daniela Traini[b], Paul M. Young[b], Patrick T. Spicer[c,*]

[a] Microstructured Fluids Research, Procter & Gamble Co., Cincinnati, OH, USA
[b] Woolcock Institute of Medical Research and Discipline of Pharmacology, Sydney Medical School, Glebe, Australia
[c] UNSW Sydney, School of Chemical Engineering, Sydney, Australia

ARTICLE INFO

Article history:
Received 22 June 2017
Received in revised form 11 January 2018
Accepted 20 January 2018
Available online xxxx

Keywords:
Emulsion
Crystallization
Microfluidic
Shape

ABSTRACT

Oil-in-water emulsion droplets, containing an elastic endoskeleton that holds the droplets in various non-spherical shapes, are formed by crystallizing a portion of the oil phase into a network of wax crystals. Such structures have recently been found to provide enhanced active ingredient delivery and shape-changing responsiveness, but robust methods of producing such droplets are needed that enable control of droplet size and shape. A continuous microfluidic flow is used here to produce endoskeleton droplets whose size is controlled by fluid flow rate and whose shape is varied between spheres, ellipsoids, and rods by control of exit temperature. A wide range of anisotropic shapes is produced using a single flow channel geometry by allowing the endoskeleton droplet to relax its deformation by varying degrees in response to fluid interfacial tension. Flexible production of shaped endoskeleton droplets will expand their application in enhanced delivery, deposition testing, and additive manufacturing processes.

1. Introduction

Complex colloidal and supracolloidal particles with anisotropic shapes have been proposed as a way to design next-generation drug delivery vehicles, [1] control self-assembly [2], and, more generally, to design colloidal particles for specific functions [3]. The examination of custom-shaped colloids has moved from the realm of single-particle experiments to production of numerous monodisperse particles [4] as a result of innovative developments in molding [5] and microfluidics [6–9].

Droplet-based microfluidic techniques can produce complex colloids using uniform single or multiple emulsions as templates for solids like Janus particles [10], armored droplets [11–13] and bubbles, [14] liquid crystals [15], and differently-shaped microcapsules and colloidosomes [16]. However, many active ingredients in drug [17], food [18], laundry [19], and cosmetic [20] products need to remain in liquid droplet form for targeted delivery [21] to tissue, hair, and fabric substrates. Solidification processes that preserve a unique particle shape also lose droplets' ability to interact with surfaces by coalescence or wetting.

Recent work [22] showed that the yield stress of internal elastic microstructures, or endoskeletons, can arrest coalescence and preserve non-spherical droplet shapes, like rods [23], by balancing the interfacial Laplace pressure. The increased collision area of elongated droplets enhances their deposition onto substrates from a fluid flow, an application that was recently patented for personal cleansing and shampoo products [24]. Weakening the yield stress or increasing interfacial tension causes non-spherical droplets to collapse, change shape, and even wrap around nearby surfaces in response [23,25]. As consumer product use is often followed by a rinsing step, increasing interfacial tension, the shape change of anisotropic droplets has also just been patented as a way to enhance retention of droplets deposited on a surface [26].

Although spherocylindrical endoskeleton droplets have only been studied individually, dispersions of flattened cylindrical droplets have been made in microfluidic channels [27,28] and flattened droplets have been made by interfacial impact [29], yielding materials monodisperse in size and shape. However, little is known about the optimal needs for droplet shape in many applications, especially when shape-change is required, so a means to produce endoskeleton droplets with more robust control over shape is needed. Changing the shape of droplets molded in a microfluidic flow typically requires changes to the microchannel dimensions.

Another approach, explored here, is to allow the endoskeleton droplets to morph into a unique shape, once they exit a flow

* Corresponding author.
E-mail address: p.spicer@unsw.edu.au (P.T. Spicer).

https://doi.org/10.1016/j.powtec.2018.01.050
0032-5910/

channel, based on the instantaneous balance of stresses on the drop. Endoskeleton droplets adjust their aspect ratio in response to a reduction in their yield stress, forming shapes with lower curvature and interfacial pressures [25]. Such an effect suggests a way to continuously tune droplet shape, and size, over the course of a microfluidic experiment. Controllably producing more complex distributions of sizes and shapes enables targeted delivery to a broad range of target geometries, such as lung surface tissue [30,31], and would also aid large-scale production of shaped droplets where dynamic shape adjustment occurs in flow [32].

In this work, we show how various spherocylindrical endoskeleton droplet shapes can be produced by a single microfluidic device using only changes in the operating conditions. Variations in fluid flow rates are used to control droplet size in the entry region of the device, where temperatures are higher than the melting point of the droplet's elastic microstructure. Channel exit temperature controls droplet shape by solidifying a specific fraction of the shape-preserving endoskeleton, arresting collapse of the droplet at a certain shape. The dynamic nature of the internal elastic network enables shape adjustment to occur after droplets are made, without losing all droplet shape anisotropy. Shapes can be produced with different dimensions than the channel used to make and mold the droplets, and subsequent solidification preserves their shape. This work expands the number of shapes possible for endoskeleton droplets and studies the limits on their consistent production. Structured emulsions enable new applications by combining the elements of shape and orientation, usually achieved only with solid particles, with the wetting and interaction behavior of liquid droplets.

2. Experimental details

Endoskeleton droplets were made of a mixture of hexadecane (99%, Sigma Aldrich) and petrolatum (Unilever). The rheological measurements of the wax-oil mixture were performed in the linear viscoelastic regime by oscillatory experiments using a TA-AR2000 rheometer in strain controlled mode at a strain of 0.1% and frequency of 1 Hz. The rheology of the mixture was characterized by measurement of the viscous modulus, G", and the elastic modulus, G'. The values of the viscoelastic moduli indicate the contribution of viscous, or fluid-like, behavior relative to elastic, or solid-like, behavior, respectively, during deformation. Droplets need a value of G' large enough to offset the interfacial tension and maintain a stable, non-spherical, shape [22]. The oil-wax mixture exhibited no elasticity above ~ 45 °C and was an easily handled Newtonian fluid at such temperatures, as shown in Fig. 1. When cooled below 45 °C, however, the viscosity and elasticity of the mixture rapidly increased as solid wax particles crystallized out of solution. A key transition temperature is 40 °C, where elasticity begins to dominate viscous behavior of the mixture during cooling based on the dominance of G' over G" in Fig. 1. We expect arrested shapes to form and be increasingly significant at temperatures below 40 °C. Droplet oil phase solid content is zero at high temperatures, because of mutual solubility; while room temperature droplet solid content can be varied between 10% and 50% based on the hexadecane:petrolatum ratio used.

Emulsion droplets were produced using a glass microfluidic chip (Dolomite 3000436) with rectangular channels 300 μm wide and 190 μm deep arranged in a T-junction geometry. At the junction, the channel width is reduced to match its depth as shown in Fig. 2. The droplets were formed at a temperature of ~ 70 °C in an aqueous 10 mM SDS (99%, Fluka) solution. Imaging of static droplet size and shape was carried out using a Moticam 10 MP camera on a Motic AE31 inverted light microscope. High-speed imaging utilized a Phantom v7.3 camera on the same microscope. Image analysis was performed using ImageJ [33] to quantify size and shape parameters by comparison with standard calibration slides. All images were

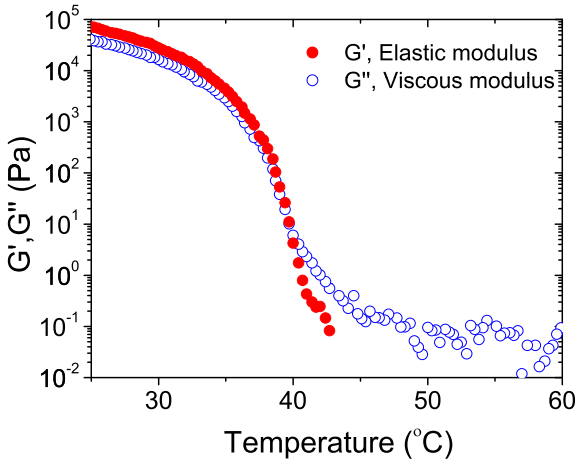

Fig. 1. Rheology of wax-oil mixture containing 35% solids as a function of temperature showing the steep increase in viscosity and elasticity as a result of crystallization of high molecular weight components of the wax near ~ 45 °C.

obtained using the Motic 10 MP except for Fig. 6a, that required the Phantom v7.3 operated at 10,000 frames/s.

The microfluidic chip was held by a metal chip holder (Dolomite 3000155) that, in conjunction with two linear connectors (Dolomite 3000024), supplied oil and aqueous phases to the chip. The flow of fluids in the chip was controlled by two Teledyne ISCO temperature-controlled syringe pumps. For the continuous water phase, a 500D pump module was used to achieve typical flow rates of 5–500 μL/min, while for the oil phase a 65DM pump module was used to achieve flow rates of 1–50 μL/min. The connectors and the chip can operate below 3 MPa and 100 °C while both pumps can operate below 25 MPa. Fluids moved from the pumps to the microfluidic chip through PTFE tubing with 0.5 mm internal diameter. The chip was placed on top of a hot plate and held at ~ 70 °C while the fluids in the syringe were kept at 70 °C by an external water circulation system. Tube length between pump and chip was kept below ~5 cm and the tube was held close to the hot plate to prevent cooling and premature structure formation.

Once the droplets were formed in the microfluidic chip, they traveled downstream from the junction and through a circular profile outlet tube (PEEK, Kinesis) whose internal diameter was selected from the range 75–500 μm based on the desired emulsion shape and

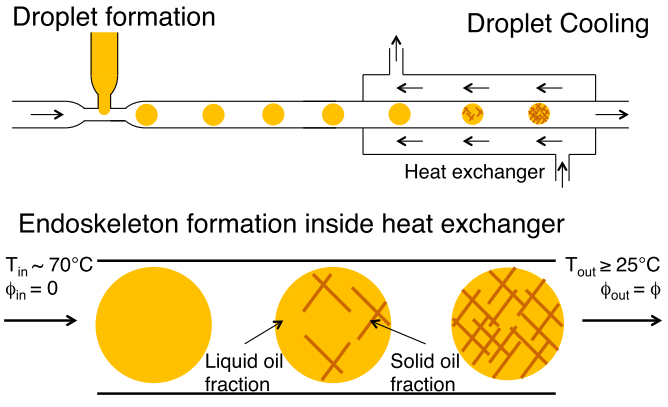

Fig. 2. Microfluidic setup used to produce structured droplets. In the first stage, oil droplets are formed in a T-junction at ~ 70 °C. Subsequently the droplets are transferred to a plastic tube and cooled in a heat exchanger down to a temperature of ~ 25 °C.

dimension. The outlet tube, ~20 cm in length, passed through a simple countercurrent tube-in-tube heat exchanger of length ~10 cm that controlled temperature via cool water circulation in the outer tube. Once produced, the structured particles were collected in a low yield stress surfactant solution, 10 mM SDS and 0.5% microfibrous cellulose, MFC (CP-Kelco), that prevented particle creaming and aggregation without affecting drop shape formation.

3. Results and discussion

3.1. Microfluidic production of spherical endoskeleton droplets

Monodisperse endoskeleton droplets are prepared with a two-step microfluidic process. The first step produces molten spherical emulsion droplets at ~ 70 °C using a temperature-controlled microfluidic device. The second step cools the emulsion droplets down to ≥ 25 °C during the ~10 ms residence time in the outlet tube and triggers crystallization of the high-melting components of the oil phase, as seen in Fig. 2. A highly porous, percolated network of very thin solid crystals forms within the droplet volume [22] and the droplet either remains spherical or adopts an anisotropic shape imposed by confinement in the outlet tube [23].

The monodispersity of the structures produced is clear in Fig. 3, where several structured droplets are arranged in a 2D hexagonal lattice at a liquid-air interface. The microfluidic process enables control of droplet radius between 40 and 200 μm by varying the relative flow rates of the oil and aqueous phases [34]. Table 1 shows the range of fluid flow rates used to obtain the different-sized droplets in this study and is consistent with previous work on the use of relative dispersed, Q_d, and continuous, Q_c, phase flow rates to change flow regime [35].

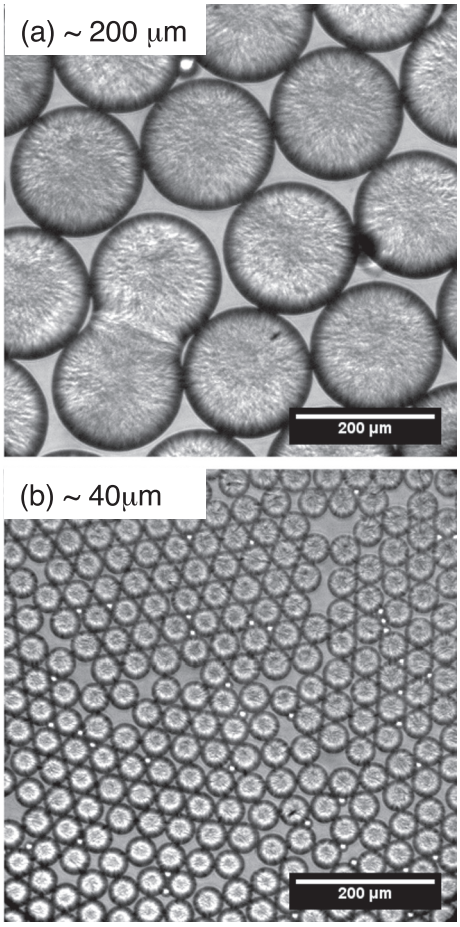

Fig. 3. Hexagonally packed emulsion droplets, containing 35% w/w crystalline solids, at the air-water interface of a sessile drop. The two images show the different sizes obtained under different flow conditions. (a) For larger droplets produced at an aqueous (continuous) flow rate of 500 μL/min and an oil (dispersed) phase flow rate of 10 μL/min, a doublet structure formed via arrested coalescence is clearly visible. (b) For smaller droplets produced at an aqueous (continuous) flow rate of 500 μL /min and an oil (dispersed) phase flow rate of 1 μL/min, some smaller daughter droplets are also visible.

Table 1
Volumetric flow rates for the dispersed, Q_d, and continuous, Q_c, fluid emulsion phases, as well as the spherical diameter, d, obtained during microfluidic production of molten hexadecane-petrolatum droplets.

Q_d(μL/min)	Q_c(μL/min)	d(μm)
5	250	87
10	250	100
50	250	200
1	500	40
10	500	200

3.2. Multiple-droplet structures based on assembly of spherical building blocks

Endoskeleton droplets retain the ability to fuse with other droplets, by initiating coalescence that is then arrested by the elastic endoskeleton at intermediate stages [22,36]. When coalescence is arrested, the resulting anisotropic structures can retain their shape indefinitely as a result of the balance between interfacial forces and internal elasticity [36]. Fig. 3a contains an example of an arrested doublet structure whose coalescence has been halted at an early stage. Inside all of the droplets the endoskeleton is visible as an array of bright anisotropic crystalline shapes under this partially polarized light. For the arrested doublet structure in Fig. 3a, the bright equatorial band in its middle is evidence of the original boundary between the two drops where the coalescence process began but was halted by the skeleton's elasticity. The alignment of the anisotropic crystals,

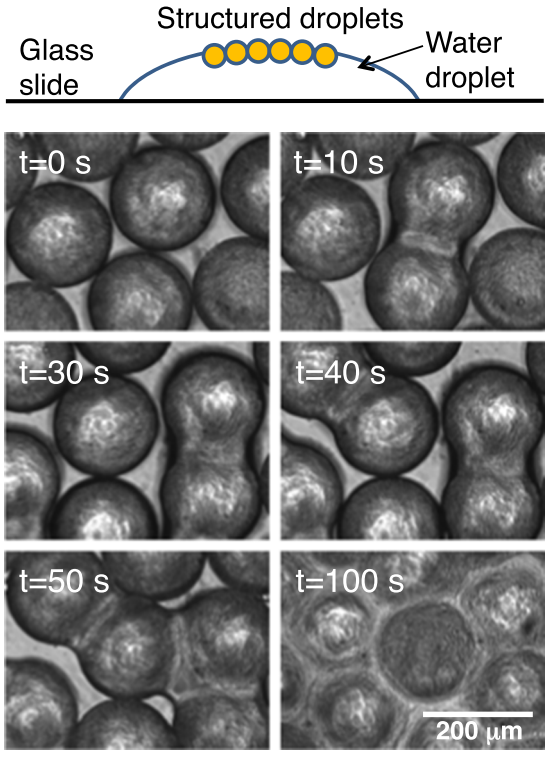

Fig. 4. Sequential spontaneous arrested coalescence of endoskeleton droplets, containing 35% w/w crystalline solids, held at the air water interface at ~ 35 °C.

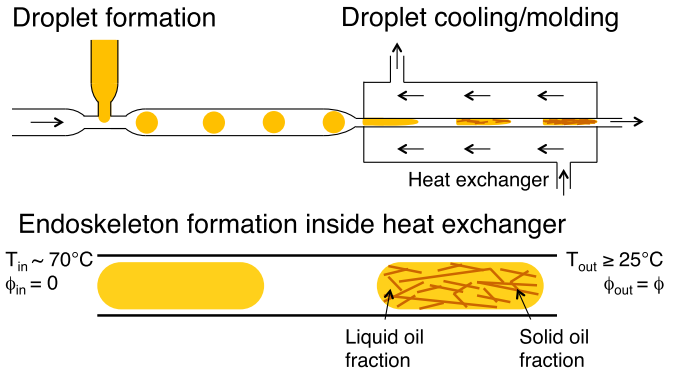

Fig. 5. Microfluidic setup used to produce structured anisotropic emulsion droplets. In the first stage, molten oil droplets are formed in a T-junction at ~ 70 °C. Subsequently, droplets pass through a smaller diameter plastic tube, that deforms them, and then are cooled to ≥~ 25 °C to form the elastic endoskeleton.

by the flows occurring during initiation and arrest of coalescence, causes the brightness maximum in the neck region. The gap on either side of the doublet causes deviation from the hexagonal close packing of the surrounding drops. The arrested structure occupies less space than two individual droplets because the interfacial pressures deform the coalescing structure. Pawar et al. [22] showed that the deformation is a useful measure of the relative strength of droplet elasticity and interfacial pressure. Doublet deformation can be quantified by calculating the strain, ϵ, defined as the difference between the length, L, of the doublet and the initial length of the two starting droplets, L_0, normalized by L_0: [22].

$$\epsilon = \frac{L_0 - L}{L_0} \tag{1}$$

For the doublet in Fig. 3a, the $\epsilon \sim 10\%$, in good agreement with previous studies of arrested doublets of this type [22]. Fig. 3b shows smaller droplets produced at a higher dispersed phase flow rate and further highlights the monodispersity possible for most of the droplets produced prior to molding. Clearly the crystallization process does not interfere with production of consistent emulsion droplets, despite the formation of internal anisotropic crystals and the resulting changes in droplet rheology and viscoelasticity.

Increasingly complex multiple-droplet structures can be formed by sequential combination of spherical structured droplets. Coalescence can be triggered by selectively heating droplets, [37] that are sufficiently close to contact one another, to ~ 35 °C. Fig. 4 shows the gradual arrested coalescence of multiple structured droplets over the course of 100 s for drops partitioned at the liquid-air interface of a sessile water droplet. The elasticity of the microstructure is reduced as a result of heating to ~ 35 °C, in the middle of the melting range determined from Fig. 1. In Fig. 4, the gradual linking of all the droplets in the field of view occurs as a result of buoyancy forces pushing the structured droplets toward the center of the curved liquid-air interface. Initially, doublets form in the second (t = 10 s) and fourth images (t = 40 s), followed by a quaternary structure in the fifth image (t = 50 s), until a single percolated structure remains that preserves the spherical character of the building blocks and reflects close packing of spheres. At lower temperatures, droplets can be assembled by providing sufficient stress to overcome the inherent disjoining pressure of the drops [38]. Uniform-sized endoskeleton droplets offer a way to study arrested coalescence structures and better model realistic structure formation in foods and coatings, where complex microstructures can arise because of the unique dynamics of arrest and restructuring [39,40]. The spherical structured droplets produced here can be thought of as flexible building blocks of anisotropic structures, because of their endoskeleton's unique ability to hold a shape.

The principles of droplet formation and emulsion creation used here are not unique to the model oil-wax system used. Such a flexible and modular route to anisotropic colloids should be possible with a large range of materials, so long as a material containing a porous elastic microstructure of tunable strength can be emulsified in a continuous liquid phase. The microfluidic process provides control over the size of the droplets and the temperature history of the endoskeleton structure, easily allowing production of milliliter quantities of structured droplets.

3.3. Microfluidic production of rod-shaped endoskeleton droplets

With a slight modification of the microfluidic setup used to fabricate structured spheres, we are also able to produce anisotropic rod-shaped emulsion droplets. The only variation in the experimental setup is a reduction of the outlet tube inner diameter, or ID. Reducing the ID below the diameter of the preceding channels containing spherical droplets creates a constriction that increases the aspect ratio of a droplet as it passes through [6], as shown in the schematic in Fig. 5.

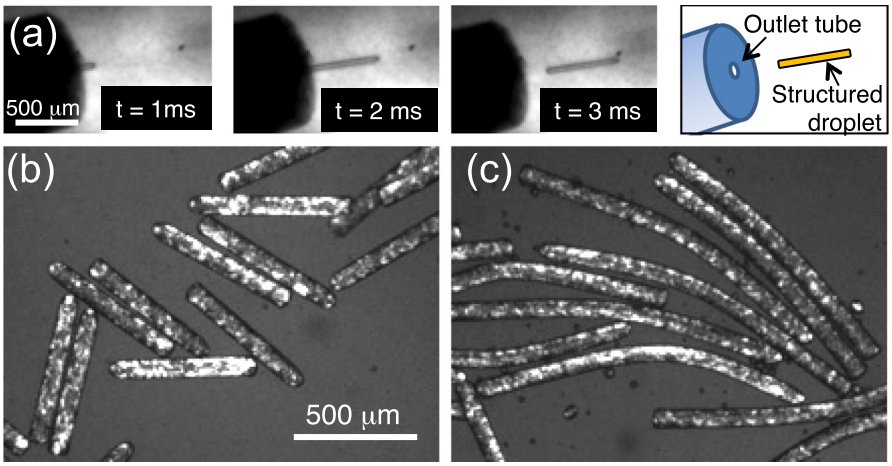

Fig. 6. (a) Four sequential images show a structured rod-shaped emulsion droplet exiting the microfluidic device at high speed. (b) Rods with diameter 75 μm and length 600 μm, produced at 25 °C and 5 μL /min oil and 250 μL /min water flow rates. (c) Rods with diameter 75 μm and length 1500 μm produced at 10 μL/min oil and 250 μL/min water flow rates. All rods contain 35% w/w crystalline solids.

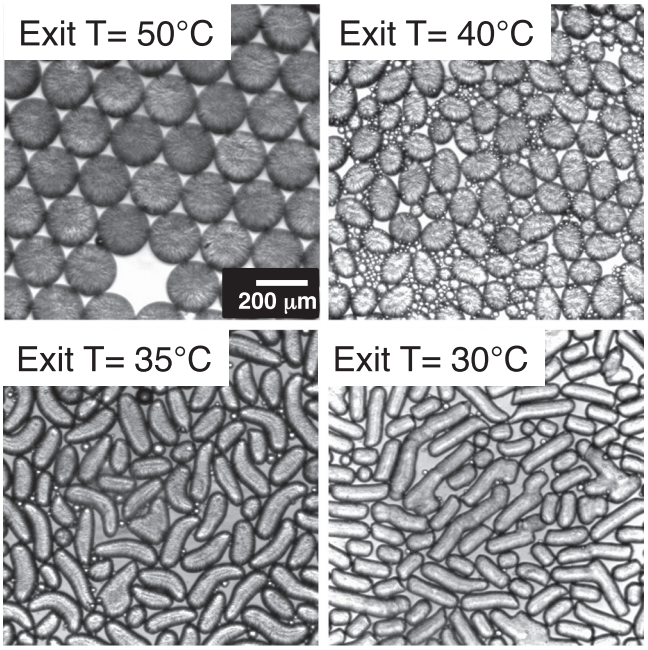

Fig. 7. Various structured anisotropic emulsion droplets produced by cooling to different final temperatures during the molding stage. Here all rods are made using flow rates of 50 μL/min for oil and 250 μL/min for water to increase production rates.

For the chip used here, when the outlet tube diameter is 100 μm, and the molten droplet diameter is larger, elongated droplets are produced. In the outlet tube, cooling forms the endoskeleton in a shape that matches the deformed emulsion under flow and preserves that shape against interfacial [23] and hydrodynamic stresses [13]. An example of droplet production in the apparatus of Fig. 5 is shown in Fig. 6a, where high-speed imaging captured three frames of an endoskeleton droplet, emerging from the exit channel, with a spherocylindrical shape whose smallest dimension matches that of the channel ID. A closer view of droplets produced in this process is shown in Fig. 6b and c. Two types of rods are produced with excellent monodispersity in size and shape, and both have the same radius of 37.5 μm as a result of their formation in a 75 μm ID channel. However, the length of the droplets is more than doubled when the aqueous continuous phase flow rate is halved. While the shorter rods are perfectly straight, the longer rods are partially bent as a result of interfacial compressive stresses and, potentially, buckling, although the anisotropy is nicely preserved. Fig. 6 also highlights the presence of a crystalline endoskeleton in each droplet, visible as bright spots in the two polarized light images.

Our qualitative observations of final droplet structures can be rationalized if we recall the theoretical model proposed to explain arrested coalescence of spherical structured droplets [22] and the one developed to design rod-shaped droplets by individual molding [23]. The ability to maintain anisotropic shapes is explained by a simple balance between interfacial and elastic forces. For an idealized spherocylindrical droplet, the compressive interfacial stress, σ_i, due to the interfacial tension, γ, should be of the order of the Laplace pressure applied by the two semi-spherical end caps with radius R_{cap} on the cylindrical section. As a result, stable anisotropic structures should be obtained when the rod radius is larger than: [23]

$$R_{cap}^{min} = \frac{2 \cdot \gamma}{\sigma_y} \quad (2)$$

where σ_y is the droplet yield stress. Eq. (2) provides a criterion for a balancing of interfacial forces with the yield stress of the endoskeleton, which can then maintain its shape by keeping the liquid interface deformed. When $\sigma_y < \sigma_i$, the endoskeleton structure yields and the particle shape relaxes toward more compact shapes [23].

Structured droplets with $R_{cap} < R_{cap}^{min}$ are not expected to maintain their original anisotropic shape, because the elastic structure will reshape to form a more compact one. Eq. (2) predicts a minimum cap radius of ~ 30 μm for rods with solids weight fraction $\phi = 0.35$ and $\sigma_y \sim 100$ Pa in a 10 mmol/L SDS solution with $\gamma \sim 1.5$ mN/m [23,25]. The prediction is consistent in magnitude with the observed stable rods with a cap radius of $R_{cap} = 37.5$ μm seen in Fig. 6.

All of the rods in Fig. 6 exit the channel at a temperature of 25 °C, so the majority of solids have been crystallized based on the rheology result in Fig. 1. An increased exit temperature will then reduce the crystalline solids present and weaken the structure's resistance to interfacial compressive stresses. Such a mechanism offers a means of controlling the ultimate shape of a droplet by varying its yield stress and requiring it to reshape itself to lower the Laplace pressure experienced upon ejection. Fig. 7 shows a study of the droplet shapes produced at higher exit temperatures and flow rates than in Fig. 6b and c. An additional degree of control over droplet shape is possible when exit temperature is varied, producing yield stresses that allow varying degrees of subsequent collapse/reshaping after the droplet exits the flow channel.

We define a critical droplet solids fraction, ϕ_c, and temperature, T_c, that determine whether the anisotropic endoskeleton has a sufficiently shape-preserving yield stress when the droplet exits the outlet tube. Once the droplet is collected at the tube outlet we observe different behaviors:

1. If the droplet solid fraction, ϕ, is below a critical solid fraction, $\phi_c \sim 0.25$, or the outlet temperature, T_{out}, is above a critical melting temperature, $T_c \sim 45$ °C, the droplet shape relaxes to a sphere within a few milliseconds of leaving the outlet. The anisotropic endoskeleton is unstable due to insufficient solid fraction or incomplete crystallization. The upper left image of Fig. 7 is an example.
2. When $\phi > \phi_c$ and $T_{out} \ll T_c$ we observe stable rigid rods for low aspect ratios, $AR < 10$, as in Fig. 6b, while for higher aspect ratios, $AR \sim 20$, we observe bent rods, like those in Fig. 6c or the bottom left of Fig. 7, suggesting the influence of a buckling and/or flow instability.
3. For $\phi > \phi_c$ and $T_{out} < T_c$ the droplets maintain anisotropic shapes, even after leaving the outlet tube, and anisotropy increases as the outlet temperature is decreased. Outlet temperature is thus a useful process variable for tuning the shape of structured droplets. In Fig. 7, a steady increase in droplet aspect ratio is seen with a decrease in outlet temperature as stronger skeletons are produced and they more rigidly resist the droplet interfacial pressures.

We also observe that drops made in the same device, but with solid fractions below $\phi_c \sim 0.25$, do not form stable rods because the resultant lower yield stress, $\sigma_y \sim 25$ Pa, is only predicted to support an $R_{cap}^{min} > 120$ μm. The simple model also explains the results in Fig. 7 where outlet temperature affects final droplet shape. By changing the outlet tube temperature, we change the exit yield stress of the endoskeleton. For temperatures above ~ 50 °C, based on the bulk rheological data in Fig. 1, we expect zero exit yield stress and spherical droplet formation. As the outlet temperature is lowered, the exit yield stress gradually increases and we observe decreasing rod end cap radius and increasing shape anisotropy stability in Fig. 7. Some rods have clearly coalesced to some extent, increasing width of the

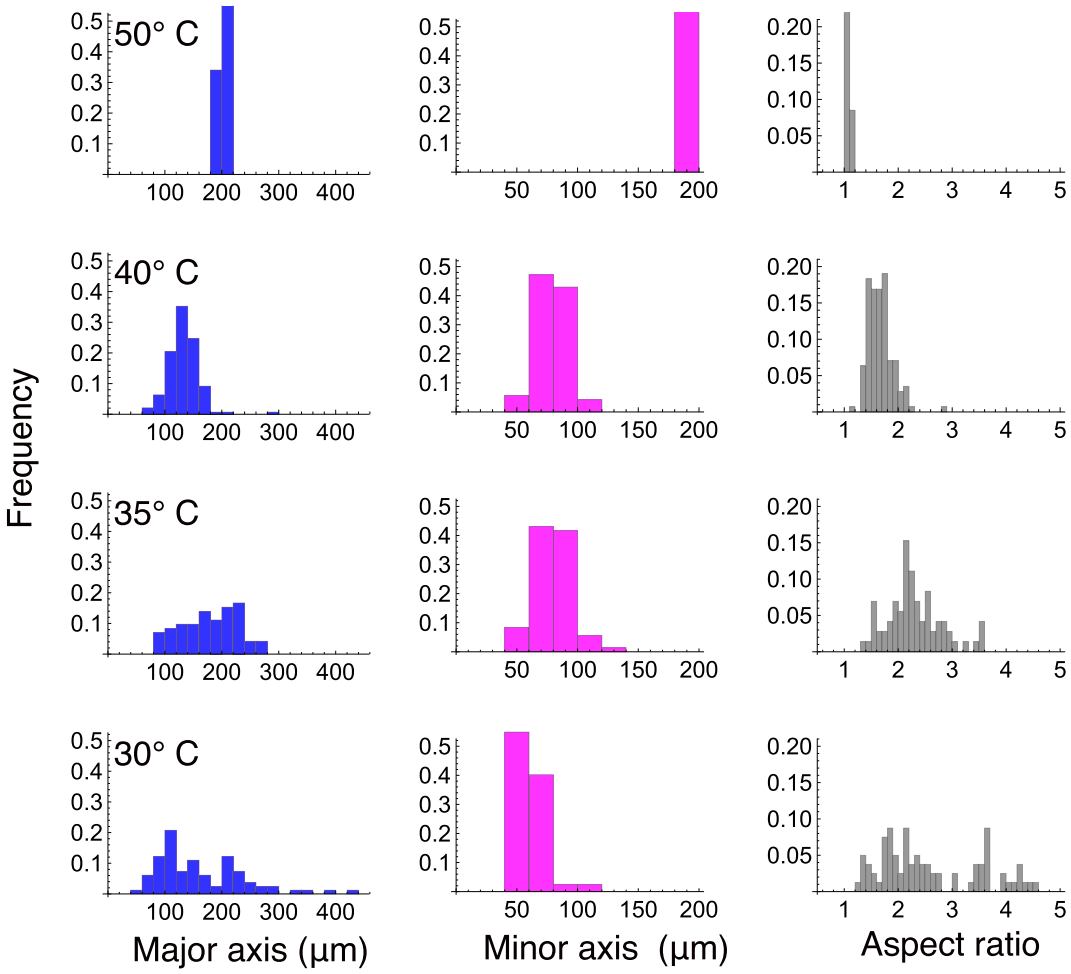

Fig. 8. Size and shape relative frequency distributions of >200 droplets in Fig. 7 and other fields of view. The droplets become increasingly polydisperse in major axis and aspect ratio as channel exit temperature is lowered, and the minor axis dimension decreases steadily toward the size of the exit channel tubing of 75 μm as the droplet shape transitions from spheres, to ellipsoids, to rods.

drop size distribution and verifying that the droplets retain a liquid interface.

Frequency distributions of droplet major and minor axes, as well as aspect ratio, are plotted in Fig. 8 for multiple, non-overlapping, fields of view, to yield populations >200, of the particles seen in Fig. 7. The droplets are relatively monodisperse in size and shape at the extreme temperatures of T_{out} = 25 °C and 50 °C as a result of a total loss of structure, at high temperatures as in Fig. 7, or the greatest ability to preserve structure at low temperatures, as in Fig. 6. As exit temperature is decreased over the intermediate range, Fig. 7, the droplets become more polydisperse in size and shape, and their aspect ratio steadily increases as anisotropy grows, as seen in Fig. 8. Although a less controlled process, the ability to vary shape by simply varying exit temperature in the same flow system enhances our ability to apply these droplets and study shape effects a number of ways.

Fig. 9 summarizes the shapes and characteristics of endoskeleton droplets produced in the microfluidic process studied here. Different exit temperatures vary the droplet solids content, producing different yield stresses that either collapse completely under interfacial pressures or adjust their shape to a more compact anisotropic configuration. The wide variation in size and shape possible in such an experiment means the two variables could be continuously varied over the course of a production run, either to yield a prescribed mixture of shapes and sizes or to continuously vary size and shape for some downstream test of performance, like deposition.

4. Conclusions

This work demonstrates the microfluidic production of endoskeleton droplets by making emulsion droplets at high temperature, shaping them by reducing outlet internal diameter, and then reducing temperature to form endoskeletons. The droplet size can be controlled by adjusting fluid flow rates, producing larger droplets when a higher relative oil flow rate is used, for example. Exit temperature can be adjusted to preserve a non-spherical elongated shape to varying degrees, upon release, depending on the balance between interfacial pressure and elasticity. Droplet deformation, controlled by geometric parameters, is arrested at a given shape by the elastic properties of the droplet skeleton and the anisotropic shape is permanently maintained. When fully crystallized, different aspect ratios can be obtained by varying the relative fluid flow rates. Non-spherical structured droplets still possess properties of spherical structured droplets, such as the possibility to wet a substrate or undergo arrested coalescence.

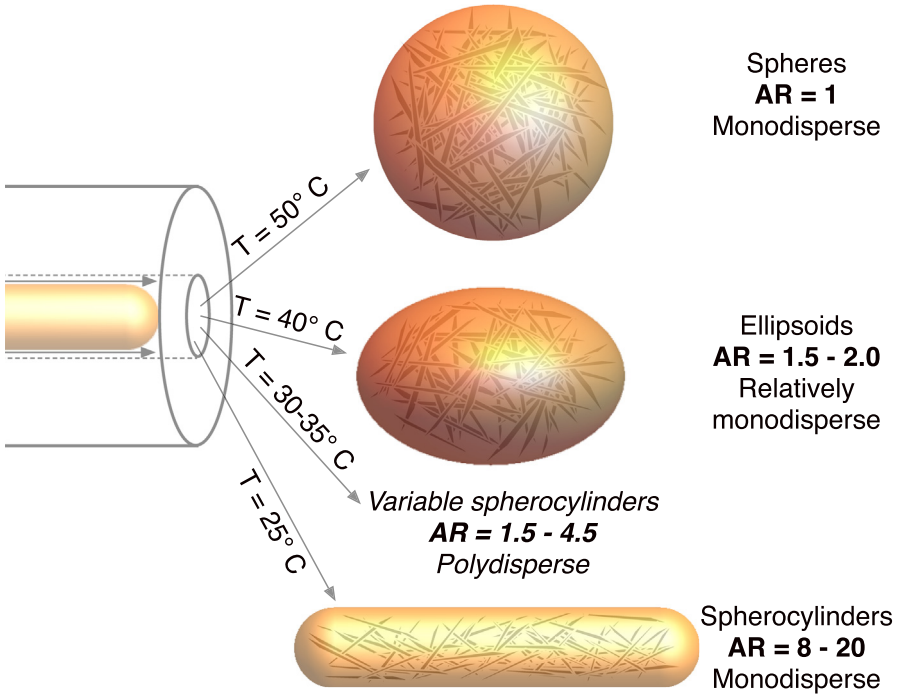

Fig. 9. Schematic summarizing the range of shapes produced, following collapse, rearrangement, or stability of shapes after ejection from a microchannel, based on the results in Figs. 6 and 7.

The microfluidic system can ease production of numerous shaped droplets and enable focused studies of shape effects in areas like inhalation, spraying, surface coating, and additive manufacturing. The droplets produced here, in the range of 50–150 μm, are appropriate for a number of industrial processes and formulations [24,26], but much smaller droplets are of interest for other applications. For example, aerosol delivery of respiratory treatments via inhalation requires droplets with much smaller dimensions, 1–5 μm, for deep lung delivery, [41] but such tiny droplets will require much stronger endoskeletons in order to resist the high Laplace pressures operating on such highly curved interfaces [23]. The lowest dimension currently possible for this system appears to be on the same order as the 10 μm thickness of the flat spherocylinders studied by Prileszky et al. [28]. More work is needed to make stable endoskeleton droplets one order of magnitude smaller, and this is a future goal of our work.

Acknowledgments

DT, PY, and PS acknowledge support by ARC Discovery Grant DP150100865. We also gratefully acknowledge the insights into the rod-shaped droplet behavior gained from Alexandra Bayles (UC Santa Barbara), Tamas Prileszky (U. Delaware), and Eric Furst (U. Delaware).

References

[1] S. Mitragotri, J. Lahann, Physical approaches to biomaterial design, Nat. Mat. 8 (1) (2009) 15–23.
[2] M. Grzelczak, J. Vermant, E. Furst, L. Liz-Marzán, Directed self-assembly of nanoparticles, ACS Nano 4 (7) (2010) 3591–3605.
[3] S. Glotzer, M. Solomon, Anisotropy of building blocks and their assembly into complex structures, Nat. Mat. 6 (2007) 557–562.
[4] D. Bartolo, D. Aarts, Microfluidics and soft matter: small is useful, Soft Matter. (2012) 1–6.
[5] T. Merkel, K. Herlihy, J. Nunes, R. Orgel, J. Rolland, J. DeSimone, Scalable, shape-specific, top-down fabrication methods for the synthesis of engineered colloidal particles, Langmuir (2009) 557.
[6] S. Xu, Z. Nie, M. Seo, P. Lewis, E. Kumacheva, H. Stone, P. Garstecki, D. Weibel, I. Gitlin, G. Whitesides, Generation of monodisperse particles by using microfluidics: control over size, shape, and composition, Angewandte Chemie. 117 (5) (2005) 734–738.
[7] D. Dendukuri, D. Pregibon, J. Collins, T. Hatton, P. Doyle, Continuous-flow lithography for high-throughput microparticle synthesis, Nat. Mat. 5 (5) (2006) 365–369.
[8] P. Panizza, W. Engl, C. Hany, R. Backov, Controlled production of hierarchically organized large emulsions and particles using assemblies on line of co-axial flow devices, Colloid Surf. A 312 (1) (2008) 24–31.
[9] J. Kim, S.A. Vanapalli, Microfluidic production of spherical and nonspherical fat particles by thermal quenching of crystallizable oils, Langmuir 29 (39) (2013) 12307–12316.
[10] Z. Nie, W. Li, M. Seo, S. Xu, E. Kumacheva, Janus and ternary particles generated by microfluidic synthesis: design, synthesis, and self-assembly, J. Am. Chem. Soc. 128 (2006) 9408–9412.
[11] A. Subramaniam, M. Abkarian, H. Stone, Controlled assembly of jammed colloidal shells on fluid droplets, Nat. Mat. 4 (2005) 553–556.
[12] S.A.F. Bon, S.D. Mookhoek, P.J. Colver, H.R. Fischer, S. van der Zwaag, Route to stable non-spherical emulsion droplets, Europ. Polymer J. 43 (11) (2007) 4839–4842.
[13] M. Mulligan, J. Rothstein, Deformation and breakup of micro-and nanoparticle stabilized droplets in microfluidic extensional flows, Langmuir 27 (16) (2011) 9760–9768.
[14] A.P. Kotula, S.L. Anna, Probing timescales for colloidal particle adsorption using slug bubbles in rectangular microchannels, Soft Matter. 8 (41) (2012) 10759.
[15] C. Ohm, C. Serra, R. Zentel, A continuous flow synthesis of micrometer–sized actuators from liquid crystalline elastomers, Adv. Mat. 21 (47) (2009) 4859–4862.
[16] R. Shah, H. Shum, A. Rowat, D. Lee, J. Agresti, A. Utada, L. Chu, J. Kim, A. Fernandez-Nieves, C. Martinez, D. Weitz, Designer emulsions using microfluidics, Matls. Today 11 (2008) 18–27.
[17] D. Malik, S. Baboota, A. Ahuja, S. Hasan, J. Ali, Recent advances in protein and peptide drug delivery systems, Curr. Drug Deliv. 4 (2) (2007) 141–151.
[18] L. Sagalowicz, M. Leser, Delivery systems for liquid food products, Curr. Op. Colloid Int. Sci. 15 (2009) 61–72.
[19] M. Clauzel, E. Johnson, T. Nylander, R. Panandiker, M. Sivik, L. Piculell, Surface deposition and phase behavior of oppositely charged polyion-surfactant ion complexes. Delivery of silicone oil emulsions to hydrophobic and hydrophilic surfaces, Appl. Mat. Interf. 3 (7) (2011) 2451–2462.
[20] P. Somasundaran, S. Mehta, P. Purohit, Silicone emulsions, Adv. Colloid Int. Sci. 128-130 (2006) 103–109.
[21] J. Champion, S. Mitragotri, Role of target geometry in phagocytosis, Proc. Nat. Acad. Sci. 103 (13) (2006) 4930.
[22] A.B. Pawar, M. Caggioni, R.W. Hartel, P.T. Spicer, Arrested coalescence of viscoelastic droplets with internal microstructure, Faraday Disc. 158 (2012) 341–350.

[23] M. Caggioni, A.V. Bayles, J. Lenis, E.M. Furst, P.T. Spicer, Interfacial stability and shape change of anisotropic endoskeleton droplets, Soft Matter. 10 (2014) 7647–7652.
[24] P. Spicer, M. Caggioni, J. Lenis, A. Bayles, Non-spherical droplet, US Patent 9,597,648, Procter and Gamble Co. (Aug 2017).
[25] M. Caggioni, J. Lenis, A.V. Bayles, E.M. Furst, P.T. Spicer, Temperature-induced collapse, and arrested collapse, of anisotropic endoskeleton droplets, Langmuir 31 (31) (2015) 8558–8565.
[26] P. Spicer, M. Caggioni, J. Lenis, A. Bayles, Shape-changing droplet, European Patent EP 2909299 B1, Procter and Gamble Co. (2017).
[27] T.A. Prileszky, E.M. Furst, Crystallization kinetics of partially crystalline emulsion droplets in a microfluidic device, Langmuir 32 (2016) 5141–5146.
[28] T.A. Prileszky, E.M. Furst, Fluid networks assembled from endoskeletal droplets, Chem. Matls. 28 (11) (2016) 3734–3740.
[29] D. Lee, S.N. Beesabathuni, A.Q. Shen, Shape-tunable wax microparticle synthesis via microfluidics and droplet impact, Biomicrofluidics 9 (6) (2015) 064114.
[30] D.A. Edwards, J. Hanes, G. Caponetti, J. Hrkach, Large porous particles for pulmonary drug delivery, Science 276 (1997) 1868.
[31] T.M. Crowder, J.A. Rosati, J.D. Schroeter, A.J. Hickey, Fundamental effects of particle morphology on lung delivery: predictions of Stokes' Law and the particular relevance to dry powder inhaler formulation, Pharm. Res. 19 (2002) 239–245.
[32] T. Merkel, V. Gräf, E. Walz, H.P. Schuchmann, Production of particle-stabilized nonspherical emulsion drops in simple shear flow, Chem. Eng. Tech. 38 (8) (2015) 1490–1493.
[33] C.A. Schneider, W.S. Rasband, K.W. Eliceiri, NIH image to ImageJ: 25 years of image analysis, Nat. Methods 9 (7) (2012) 671–675.
[34] P. Garstecki, M. Fuerstman, H. Stone, G. Whitesides, Formation of droplets and bubbles in a microfluidic T-junction-scaling and mechanism of break-up, Lab Chip 6 (3) (2006) 437–446.
[35] B.R. Benson, H.A. Stone, R.K. Prud'homme, An "off-the-shelf" capillary microfluidic device that enables tuning of the droplet breakup regime at constant flow rates, Lab Chip 13 (23) (2013) 4507–4511.
[36] A.B. Pawar, M. Caggioni, R. Ergun, R.W. Hartel, P.T. Spicer, Arrested coalescence in pickering emulsions, Soft Matter. 7 (2011) 7710–7716.
[37] S. Kiokias, A. Bot, Temperature cycling stability of pre-heated acidified whey protein-stabilised O/W emulsion gels in relation to the internal surface area of the emulsion, Food Hydrocoll. 20 (2) (2006) 245–252.
[38] J. Bibette, D. Morse, T. Witten, D. Weitz, Stability criteria for emulsions, Phys. Rev. Lett. 69 (16) (1992) 2439–2442.
[39] P. Dahiya, M. Caggioni, P.T. Spicer, Arrested coalescence of viscoelastic droplets: polydisperse doublets, Phil. Trans. R. Soc. A 374 (2072) (2016) 20150132.
[40] P. Dahiya, A. DeBenedictis, T.J. Atherton, M. Caggioni, S.W. Prescott, R.W. Hartel, P.T. Spicer, Arrested coalescence of viscoelastic droplets: triplet shape and restructuring, Soft Matter. 13 (2017) 2686–2697.
[41] J.N. Pritchard, The influence of lung deposition on clinical response, J. Aerosol Med. 14 (Suppl 1) (2001) S19–26.